Heliyon 7 (2021) e07917

Contents lists available at ScienceDirect

Heliyon

journal homepage: www.cell.com/heliyon

Research article

The effects of different activating agents on the physical and electrochemical properties of activated carbon electrodes fabricated from wood-dust of *Shorea robusta*

D. Shrestha [a,*], A. Rajbhandari (Nyachhyon)[b]

[a] Patan Multiple Campus, Tribhuvan University, Patan Dhoka, Lalitpur, Nepal
[b] Central Department of Chemistry, Tribhuvan University, Kirtipur, Kathmandu, Nepal

ARTICLE INFO

Keywords:
Shorea robusta
Specific capacitance
Energy density
Power density
Cyclic stability

ABSTRACT

This study focuses on the effects of activating agents on the physical and electrochemical properties of activated carbon (AC) electrodes, fabricated from wood dust of *Shorea robusta*. Three different activating agents namely H_3PO_4, KOH and Na_2CO_3 have been used to prepare ACs, which were named as: Sr–H_3PO_4, Sr–KOH and Sr–Na_2CO_3. The ACs were characterized by TGA/DSC, XRD, Raman, SEM, FTIR and BET. All the as prepared ACs were found to be amorphous in nature. The oxygen surface functionality was developed at the surface. The surface area of Sr–H_3PO_4, Sr–KOH and Sr–Na_2CO_3 were found to be 1269.5 m^2/g, 280.6 m^2/g and 58.9 m^2/g respectively. The activated carbon-electrodes were then fabricated and supercapacitive performances were evaluated by "three electrode system" in aqueous 6M KOH using cyclic voltammetry (CV), galvanostatic charge discharge (GCD) and electrochemical impedance spectroscopy (EIS).The GCD performed at 1A/g revealed the specific capacitance values were 136.3 F/g, 42.2 F/g and 59.1 F/g for Sr–H_3PO_4, Sr–KOH and Sr–Na_2CO_3-electrodes, respectively. Energy density for Sr–H_3PO_4 electrode was found to be 3.0 Wh/kg at 99.6 W/kg power densities. Moreover, it also displayed imposing cyclic stability of about 96.9 %, 89.5 % and 78.5 % after 1000 cycles of charge/discharge respectively. The overall electrochemical performance of Sr–H_3PO_4 showed outstanding supercapacitive performances demonstrating the high possibility of this material to be used for the EDLC application in supercapacitive energy storage. The Nyquist plot also showed the lowest internal resistance of about 0.4 Ω for Sr–H_3PO_4 electrode.

1. Introduction

The storage of energy shows a key role in achieving global energy demand and sustainability. To till date, various energy storage devices have been established, like solar cell, fly wheel, compressed air, fuel cell, supercapacitor and battery [1, 2]. Among them, supercapacitors and batteries have been proven to be the most effective and promising electrochemical energy storage devices for practical application [3] due to their excellent power density, outstanding pulse charge-discharge performance, superior lifespan and low maintenance cost [4]. Based on charge storage mechanisms, supercapacitors may be (i) electrical double layer capacitors (EDLC) or (ii) pseudo-capacitors [5]. For supercapacitors, conducting polymers and carbon-based materials have been regarded as the most promising materials [6, 7, 8, 9]. They are generally prepared from lignocellulosic materials that consisted of high percent of carbon and low inorganic content as well [10, 11, 12, 13] and are considered to have a huge potential in improving the electrode performance in supercapacitors [14, 15, 16]. Various biomass precursors have been chemically treated and carbonized into activated carbons for supercapacitors such as cherry stone [17], fish scale [18], waste paper [19], water bamboo [20], yeast cells [21], pine-cone [22], willow catkins [23], celtics leaves [24], waste tea-leaves [25], sunflower seed shell [26], ginkgo shells [27], cow dung [28], human hair [29] and sewage sludge [30]. The use of these materials in electrochemical performances are due to large specific surface area, pore size distribution and pore volume [31]. Such type of characteristic properties could be obtained by activation of the precursor. Two types of activation techniques are generally employed: physical activation and chemical activation.

In physical activation, precursor is carbonized at high temperatures by passing oxidizing gases like CO_2, H_2O vapors whereas in chemical

* Corresponding author.
E-mail address: shresthadibyashree@gmail.com (D. Shrestha).

https://doi.org/10.1016/j.heliyon.2021.e07917
Received 30 June 2021; Received in revised form 11 August 2021; Accepted 1 September 2021

activation, chemicals like $ZnCl_2$, H_3PO_4, KOH, K_2CO_3, Na_2CO_3 were used as activating agent during carbonization step [15, 16]. Chemical activation process exhibited superior to physical activation as it doesn't require high heating during carbonization. In these days, attention has been given for chemical activation to have better electrochemical performances.

Wang et al. [32] has reported, KOH as activating agent that showed better performance to obtain honeycomb like carbon foam. It exhibited a large specific surface area of 1313 m^2/g and a high specific capacitance of 473 F/g. In the same way, porous carbon was converted from natural silk via coupled activation and graphitization process, which showed a high specific surface area of 2494 m^2/g and a large pore volume of 2.28 cm^3/g. Further for supercapacitor application, the silk derived hierarchial porous carbon demonstrated a high specific capacitance of 242 F/g, a high-energy density of 102 Wh/kg, as well as excellent cycling life stability (9% loss after 10,000 cycles).

Similarly, activated carbon nanospheres was obtained after KOH activation and further post processing of coconut shells were found to have a surface area of 2000 m^2/g, total pore volume of 1.2 cm^3/g, specific capacitance of 250 F/g in 1M H_2SO_4 electrolyte. 93% capacitance retention was observed after 2000 cycles [33]. Correspondingly, Molina-Sabio et al. has studied the carbon sample obtained after the processing of sunflower seed shell to have specific capacitance of 244 F/g in 0.1 M HCl electrolyte, surface area of 2585 m^2/g pore volume of 1.4 cm^3/g and good cycle stability [31]. Zhang et al. presented the activated carbon nanospheres obtained from carrageenan and possesses a surface area of 1704 m^2/g, total pore volume of 0.9 cm^3/g, specific capacitance of 343 F/g using KOH and CO_2 activation in 1 M H_2SO_4. And it has a cycle life of about 2500 cycles [34]. Here, KOH was applied to produce microporosity than mesoporosity [35]. In these days, attention has also given towards phosphoric acid as activating agent to produce mesopores along with micropores [31]. These highly porous carbon materials having high surface areas are considered as potential candidates for fast charge transfer and the double layer formation of electrolyte ions in the networks of the electrode [34, 36] and was reported for the preparation of electrode materials for electrical double layer capacitors (EDLC) [37, 38, 39].

In this study, it is a particular interest to select the wood dust of *Shorea robusta* (common name "Sal") as a precursor to make activated carbon (AC). *Shorea robusta* is a large tree reaching a height of 45m, belongs to the family- Dipterocarpaecea. This tree is native to the Indian subcontinent, ranging south of the Himalaya, from Myanmar in the east to Nepal, India and Bangladesh. *Shorea robusta* is distributed in the southern terrain of Nepal from east to west.

It is considered as the most valuable tree species in Nepal. Most of the rural communities of Nepal, which constitute 80% of the total population of the country depend on Sal forest for their survival [40]. The major part of *Shorea robusta* is used in carpentry and construction, and also as a main source of fuel wood. Carpentry work constitutes a major source of waste byproducts as sawdust and wood dust. These waste byproducts have high carbon content in lignocellulosic form having low content of inorganic materials and relatively high content of volatile matters. Hence, currently, attention has given to convert waste byproducts into renewable energy storage material in general and biomass energy in particular. Thus, one of the cost effective way is to convert the wood residue to activated carbon which in turn used for energy storage device.

There are tremendous efforts in finding new materials for supercapacitor application. One of the research areas is materials preparation from natural products where main focus is optimizing the conditions for obtaining high surface area porous carbonaceous material. In this study, wood dust of *Shorea robusta* was used as precursor, which was chemically activated with different activating agents namely; phosphoric acid (H_3PO_4), potassium hydroxide (KOH) and sodium carbonate (Na_2CO_3). In addition, a low carbonization temperature of 400 °C unlike higher temperature (600–800 °C) was used. Besides these, other new contribution of this study were the selection of an electrolyte to have wide voltage window, high electrochemical stability of the materials as supercapacitor electrode, high ionic conductivity as well as availability at high purity, which are most important parameters for electrode materials to be suitable for supercapacitor application. These are the originality/novelty of this study.

2. Experimental procedures

2.1. Materials and methods

The analytical grade chemicals were used as procured. Phosphoric acid (H_3PO_4), having 85% purity, was obtained from Fischer Scientific, India. Potassium hydroxide (KOH) and anhydrous sodium carbonate (Na_2CO_3) were procured from Merck specialties Pvt. Ltd. Nanoporous carbon black, Polyvinylidine fluoride (PVDF), N-methyl pyroline (NMP) were obtained from Sigma-Aldrich (USA). Wood dust of *Shorea robusta* (Sal) has been obtained from local carpentry/saw mill of Kathmandu, Nepal.

2.1.1. Synthesis of activated carbon

Wood dust of *Shorea robusta (Sal)* collected from local saw mill was washed with distilled water and dried at 110 °C for 24h. It was crushed, grinded and sieved through 150 μm sized sieve to obtain a fine powder, which was used as a precursor material for the preparation of ACs. It was followed by chemical activation. Three different activating agents, H_3PO_4, KOH and Na_2CO_3 have been used.

First of all, the fine wood dust powder was divided into three parts. The first part was impregnated with H_3PO_4, the second part was impregnated with KOH and third part with Na_2CO_3. The precursor to activating agent was taken in the ratio 1:1 (w/w), mixed thoroughly and left for 24 h at room temperature for proper soaking. Then after, the soaked samples were evaporated at 110 °C in an oven to obtain dry samples. This method is in practice for preparation of the activated carbons [41, 42, 43]. The weighed amount of impregnated precursor was introduced into the horizontal tubular furnace for carbonization at 400 °C under the continuous flow of N_2 for 3h. The tube furnace was turned off to cool down the samples maintaining inert atmosphere of nitrogen. The hot distilled water was used for washing the cooled samples for several times followed by washing with cold distilled water. The process was continued until washed water became neutral and ions of activating agents also get removed. Finally, the obtained samples were dried at 110 °C, stored and used for advanced characterization and electrochemical application. Thus obtained three different as prepared ACs were then named on the basis of activating agent and carbonization condition (Table 1).

2.2. Characterization

The pyrolytic behaviors of the raw wood dust powder were investigated by TGA/DSC (SDT Q600 V20.9 Build 20). The morphology of the as prepared ACs was determined by Scanning Electron Microscope (SEM, Nanoeye, Korea).The samples was gold coated prior to SEM observation. Phase state was evaluated by using X-ray Diffraction (XRD, Rigaku RINT 2000 Diffractometer). Similarly, surface carbon-oxygen functional groups present in samples were identified performing FT-IR measurements using FT-IR instrument (Bruker, Vertex 70, Germany). The %

Table 1. Name of as prepared ACs on the basis of activating agents and carbonization conditions.

Name of ACs	Activating agent	Carbonization temp (°C)	Carbonization time (h)	Atmosphere
Sr–H_3PO_4	H_3PO_4	400	3	N_2
Sr–KOH	KOH	400	3	N_2
Sr–Na_2CO_3	Na_2CO_3	400	3	N_2

transmission of samples was recorded over 4000-400 cm^{-1}. The presence of the amorphous ACs was confirmed by Raman signal [labRAM HR800 (JOBIN YVON)]. The surface area of the ACs was measured by BET (Micromeritics ASAP 2020 system).

2.2.1. Fabrication of activated-carbon-electrodes

In order to fabricate activated-carbon-electrodes, 8 mg of each of the three as prepared ACs (Sr–H_3PO_4, Sr–KOH and Sr–Na_2CO_3) was mixed separately with 1 mg of carbon black and 1 mg of PVDF. The carbon black was used to provide sufficient conductivity whereas PVDF acted as a binder. To disperse PVDF, 200 μL NMP solution was added to the mixture and it was grinded and mixed thoroughly. Then the mixture solution was dropped with the help of micro-pipette on 1 cm^2 Ni-foam, that acts as a current collector and dried thoroughly at 70 °C in an oven for overnight. Thus, activated-carbon-electrodes were fabricated which have been used as working electrodes.

2.2.2. Experimental set up for electrochemical characterization

The three-electrode electrochemical set up was established for electrochemical characterization in which as fabricated activated-carbon-electrodes was used as working electrode, platinum-plate was used as counter electrode and Ag/AgCl was used as a reference electrode. Here, 6M aqueous KOH was used as an electrolyte. Prior to measurement, activated-carbon-electrodes were soaked in aqueous KOH for overnight. A Metrohm Autolab (PGSTAT 302 N) potentiostat/galvanostat was used to perform electrochemical measurement. The supercapacitor performances were evaluated by (1) cyclic voltammetry (CV), (2) galvanostatic charge/discharge (GCD) and (3) electrochemical impedance spectroscopy (EIS).

For the CV measurement, a potential window of -1.0 to -0.2 V was used at the scan rates of 2, 5, 10, 20, 50 and 100 mV/s. The GCD measurement was performed at current densities of 1, 2, 3, 5, 10, 15 and 20 A/g over the same potential window as the CV measurements. The EIS was studied over the frequency range of 100 kHz to 0.1 Hz at the perturbation signal of 10 mV. The circuits of the cells were evaluated using Nova 1.1 software.

3. Results and discussion

3.1. Thermogravimetric analysis (TGA)/Differential scanning calorimetry (DSC)

TGA/DSC measurements were carried out to understand the pyrolytic behavior of the wood dust powder/precursor. Figure 1 illustrates the TG and DSC curves of raw wood dust powder of *Shorea robusta* (Sal). A slight weight loss was observed from 60-100 °C under the N_2 flow of 60 mL/min in TG curve due to dehydration. This was also obvious from a sharp endothermic peak at 100 °C from DSC. A shallow peak in TG plot at around 200–300 °C might be due to decomposition of hemicellulose which was substantially completed at 300–310 °C [23] is confirmed from DSC curve, where a slight weight loss was clearly observed in between 200-300 °C. A significant weight loss was observed in 300–400 °C from TG, which was confirmed by a sharp endothermic peak at around 390 °C of DSC. This weight loss indicates the breakdown of cellulose into components like carboxyl, lactone, lacto and carbonyl. The conversion of cellulose into organic volatile matters leading to desorption of CO_2 and CO might also be the reason for the weight loss. It exhibited that about 60% of weight loss occurs around 400 °C [35]. Samples are more stable beyond 400 °C. Therefore, 400 °C was found to be suitable for carbonization process [42].

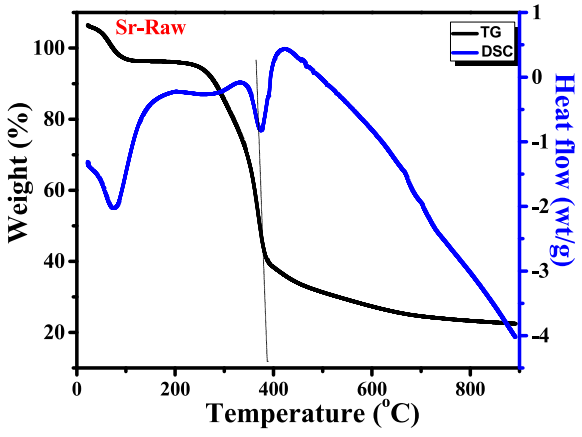

Figure 1. TGA/DSC curves of raw sawdust power (Sr-Raw).

3.2. X-ray diffraction (XRD) measurement

Figure 2 shows the XRD pattern of the as prepared ACs. The XRD pattern of raw precursor (Sr-Raw) showed peaks at around 15 and 22, 2θ degree (Bragg's angle), whereas in chemically activated carbonized samples; Sr–H_3PO_4, Sr–KOH and Sr–Na_2CO_3, those two sharp peaks were found to be disappeared completely. But broad peak was seen at around 26, 2θ degrees corresponding to (002) diffraction of the disordered stacking of the microstructures. Since no higher and sharper peak at (002) plane was seen, which confirms the absence of degree of graphitization. The broad peaks at around 20 to 30, 2θ degree indicates the presence of amorphous nature of carbon. Besides this, there was no other peaks visualized in XRD pattern which revealed that there is no any other effect of activating agents like H_3PO_4, KOH and Na_2CO_3. However, some peaks could be seen in Sr–H_3PO_4 even after careful washing, which might be due to some impurities or moisture. It is common to have some shoot off peak due to impurities from activating agent. The effect of such impurities on the performance of materials has not been substantiated yet [43].

3.3. Raman scattering analysis

Figure 3 presents the Raman spectra of as prepared ACs, which demonstrated strong D and G bands approximately at 1355 cm^{-1} and 1598 cm^{-1} respectively. Here D band at 1355 cm^{-1} indicated for disordered carbon in all as prepared ACs (Sr–H_3PO_4, Sr–KOH and Sr–Na_2CO_3). Similarly, G band was obvious in sample Sr–H_3PO_4 and Sr–Na_2CO_3 while in Sr–KOH, it was found to be small. The peak intensity ratio of G band to D band [I(G)/I(D)] provides semi quantitative information of crystallization degree of graphitic carbon in all as prepared samples. The ratio I(G)/I(D) for Sr–H_3PO_4, Sr–KOH and Sr–Na_2CO_3 was found to be 1.1, 1.1

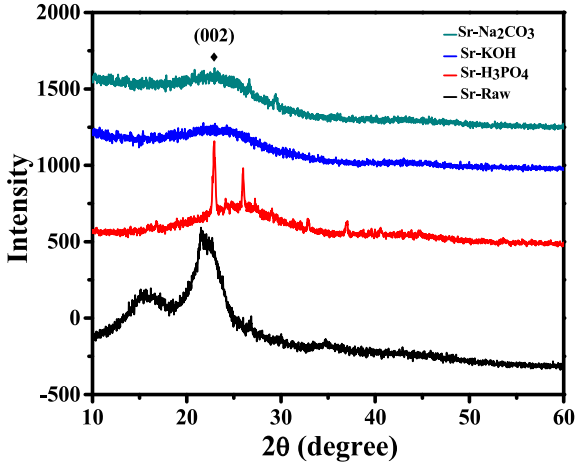

Figure 2. XRD pattern of Sr–H_3PO_4, Sr–KOH and Sr–Na_2CO_3 along with Sr-Raw.

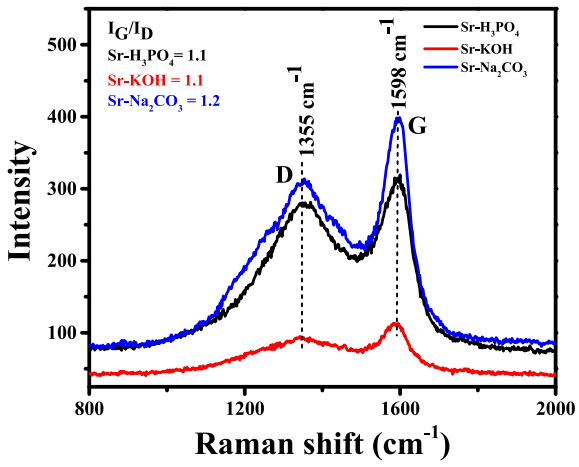

Figure 3. Raman spectra of Sr–H_3PO_4, Sr–KOH and Sr–Na_2CO_3.

and 1.2 respectively. The ratio I(G)/I(D) was found to be approximately 1 in all the ACs showing the formation of disordered carbon (amorphous carbon) [44]. The similar results have been confirmed by XRD pattern.

3.4. Fourier transforms infrared (FTIR) analysis

Figure 4 shows the FTIR spectra of Sr–H_3PO_4, Sr–KOH and Sr–Na_2CO_3. FT-IR spectra of "raw sawdust powder" of *Shorea rabusta* (Sr-Raw) showed the adsorption band at around 3331 cm^{-1} which was assigned to –OH stretching of carboxyl, phenol and alcohol vibration and adsorbed water. The presence of this band in Sr–H_3PO_4 is indicative of better functionalization of carbon. Though it looks to be disappeared from other samples but, in fact it has not disappeared rather decreased. This is due to presence of –OH group. It is also supported from thermal analysis (TGA/DSC). The TGA/DSC curve (Figure 1) clearly shows mass loss at around 100 °C, indicating evaporation of water molecules. The band at around 2942 cm^{-1} is assigned to aliphatic C–H stretching adsorption. The band at around 2333 cm^{-1} (2330-2359 cm^{-1}) is assigned for CH_3 of alkane. The broad band at 1580 cm^{-1} (in the region 1500–1900 cm^{-1}) is due to C–C vibrations in aromatic rings. Similarly, the broad band observed in the region 1000–1300 cm^{-1} is usually focused with oxidized carbon and has been assigned to C–O stretching in acids, alcohols, phenols, ethers and/or esters groups [45]. This point is also supported by TGA/DSC curve (Figure 1), which clearly shows significant mass loss between 300 to 400 °C. This is due to the breakdown of cellulose into carboxyl, lactone and lacto groups, which is due to desorption of CO_2 and CO, converting cellulose into organic volatile matters present in the sawdust [46].These results are in good agreement with the findings of many investigators [45, 46]. The FTIR spectra show that the effective functionalization of precursor by the activating agents used in this study.

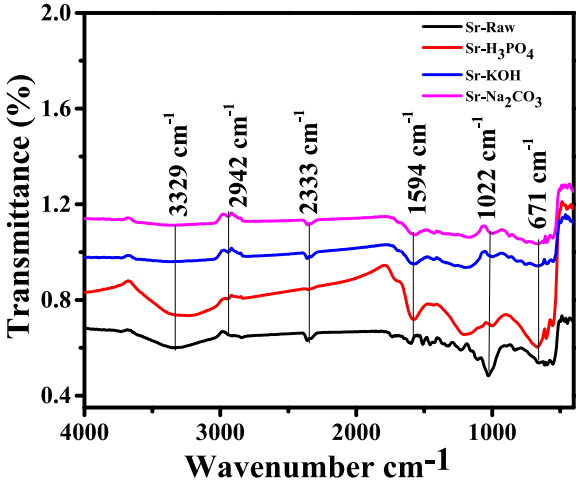

Figure 4. FTIR spectra of Sr–H_3PO_4, Sr–KOH and Sr–Na_2CO_3 along with Sr-Raw.

3.5. N_2 adsorption/desorption isotherm

Figure 5 shows the N_2 adsorption/desorption isotherms at 77 K for all as prepared ACs. As can be seen in Figure 5, the isotherms showed a drastic uptake indicating the presence of micropores at lower relative pressure region ($P/P^0 < 0.1$) in all the ACs. The uptake in lower relative pressure seems to decrease in KOH and Na_2CO_3 activated carbon samples; however, at high relative pressure, the plateau was reached. It indicates that, these ACs namely Sr–KOH and Sr–Na_2CO_3 consisted of micropores. The amount of nitrogen uptake in Sr–H_3PO_4 has increased significantly at the pressure $P/P^0 = 0.4$, showing hysteresis loop during adsorption and desorption of nitrogen. Such hysteresis loop did not exist in the adsorption/desorption curve for Sr–KOH and Sr–Na_2CO_3 samples. As the relative pressure increases up to $P/P^0 \cong 0.5$, the adsorption volume of Sr–H_3PO_4 also increased. With further increase of pressure, widely opened knees and the clear hysteresis loop were observed. This was indicative of the presence of a considerable amount of small mesopores in Sr–H_3PO_4.

The BET specific surface areas of Sr–H_3PO_4, Sr–KOH and Sr–Na_2CO_3 along with commercial carbon were calculated by BJH adsorption method which is given in Table 2. Among the three different samples, Sr–H_3PO_4 showed highest BET surface area of 1269.5 m^2/g followed by 280.6 m^2/g of Sr–KOH and 58.9 m^2/g of Sr–Na_2CO_3. It might be due to the presence of innumerable mesoporosity along with microporosity in the case of phosphoric acid activated carbon (Sr–H_3PO_4) [35]. The low surface area of Sr–KOH and Sr–Na_2CO_3 may be due to low carbonization temperature of 400 °C for KOH and Na_2CO_3 activation. As reported in literature [47, 48], the activation temperature should be > 700 °C which can react with carbon to generate pores. The SEM image of Sr–H_3PO_4 sample (Figure 6 a.) also showed clear honey comb like structure with extensive porosity.

3.6. Scanning electron microscopy (SEM) analysis

Figure 6 a-c illustrate the SEM micrographs of Sr–H_3PO_4, Sr–KOH and Sr–Na_2CO_3 at the magnification of x2.0k showing nice morphologies with pores. The evaporation of activating agents H_3PO_4, KOH and Na_2CO_3 during carbonization process leads to the pore development on

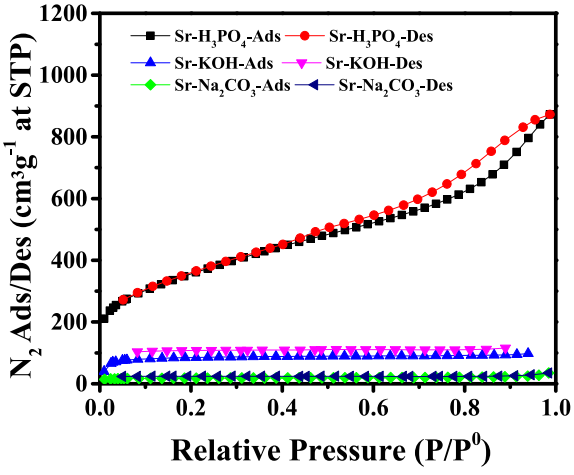

Figure 5. N_2 adsorption/desorption isotherms at 77 K for Sr–H_3PO_4, Sr–KOH and Sr–Na_2CO_3.

Table 2. BET Specific surface area of as prepared Activated Carbon samples.

Name of Sample	Specific Surface Area (m^2/g)
Sr–H_3PO_4	1269.5
Sr–KOH–4S	280.6
Sr–Na_2CO_3	58.9
Commercial carbon	876.02

the surfaces of the ACs [49]. Among them, H_3PO_4 activated carbon sample i.e. Sr–H_3PO_4, exhibited honeycomb like internal structure with well-developed pores. Among the three activating agents, H_3PO_4 is considered as the good dehydrating agent than KOH and Na_2CO_3 as in Sr–KOH and Sr–Na_2CO_3, pores are not very obvious. It may be due to low carbonization temperature for Sr–KOH and Sr–Na_2CO_3 [50]. The well-developed pores in Sr–H_3PO_4 led to high BET surface area.

3.7. Supercapacitive performances activated-carbon-electrodes

Though the surface area and porosity of Sr–KOH and Sr–Na_2CO_3 were not very satisfactory as compared to Sr–H_3PO_4, yet their electrodes (activated-carbon-electrodes) were also used for supercapacitive performances and results were compared.

3.7.1. Cyclic voltammetry (CV) studies of activated carbon electrode

Comparative CV of Sr–H_3PO_4, Sr–KOH and Sr–Na_2CO_3 electrodes and commercial carbon-electrode at 100 mV/s scan rate are shown in Figure 7. The CV at various scan rates of 2 mV/s, 5 mV/s, 10 mV/s, 20 mV/s and 50 mV/s were also obtained (not shown in figure). The CV were found to be approximately rectangular in shape which indicates the electrical double layer capacitive (EDLC) behavior. Among these three as prepared activated-carbon-electrodes, Sr–H_3PO_4-electrode, behaved well and rectangular shape (black line) was found to be comparable with commercial carbon electrode (pink line). The redox peaks were not observed in the CV however the larger loop area could be seen which is associated to high specific capacitance. Nature of such CV was evidenced for the EDLC processes which was reported in our previous study [51]. Hence, charge storage was found to be totally EDLC type. A maximum current of about 13 A/g was found which was significantly high, whereas in case of Sr–KOH-electrode and Sr–Na_2CO_3-electrode, CV were not very rectangular and current density was also found to be truncated. That's why their electrochemical capacitive behavior was deprived in comparison to Sr–H_3PO_4-electrode.

3.7.2. Specific capacitance studies of activated carbon-electrodes

The specific capacitance (C_{SP}) of activated carbon-electrodes was calculated using Eq. (1)

$$C_{SP} = \frac{I\Delta t}{m\Delta V} \quad (1)$$

where, discharge current is I (A), discharge time is Δt(s) in the potential window of ΔV(V) and the mass of active material is m (g).

The specific capacitance value of all the three as prepared activated carbon-electrodes are shown in Table 3. As can be seen, the highest specific capacitance (136.3 F/g) has been obtained for Sr–H_3PO_4 electrode, which is even higher than commercial-activated-carbon-electrode (91.6 F/g).

Figure 8 a. shows the plot of specific capacitances as a function of current density. The curve shows that there was a sharp decrease of specific capacitance with increase in current density up to 5 A/g in all three electrodes. Then after 5 A/g, specific capacitance was found to be approximately constant. The specific capacitance of Sr–H_3PO_4 electrode yielded a value of 136.3 F/g at 1 A/g and kept a value of 126.5 F/g at 2 A/g, 121.9 F/g at 3 A/g, 115.9 F/g at 5 A/g, 107.2 F/g at 10 A/g, 101.5 F/g at 15 A/g and 97.3 F/g at 20 A/g, that appeared to be much higher than other two carbon electrodes namely Sr–KOH-electrode and Sr–Na_2CO_3-electrode, which are illustrated in Table 4. Figure 8 b shows the comparison of specific conductance of Sr–H_3PO_4-electrode, Sr–KOH-electrode and Sr–Na_2CO_3-electrode - with commercial-activated-carbon at 1 A/g current density. The highest specific capacitance of Sr–H_3PO_4-

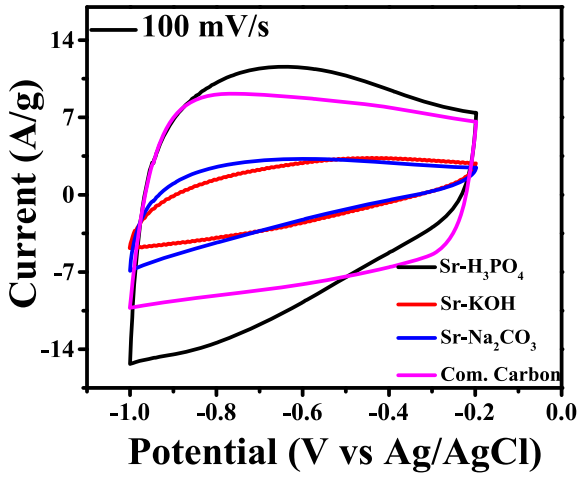

Figure 7. Comparison of CV curves of Sr–H_3PO_4, Sr–KOH and Sr–Na_2CO_3 electrodes along with commercial carbon electrode at 100 mV/s.

Table 3. Name of activated carbon-electrodes and their specific capacitance from GCD (at 1 A/g).

S.N.	Name of the activated-carbon- electrodes	Specific Capacitance (F/g)
1	Sr–Na_2CO_3-electrode	59.143
2	Sr–KOH-electrode	42.189
3	Sr–H_3PO_4-electrode	136.339
4	Commercial-activated-carbon-electrode	91.678

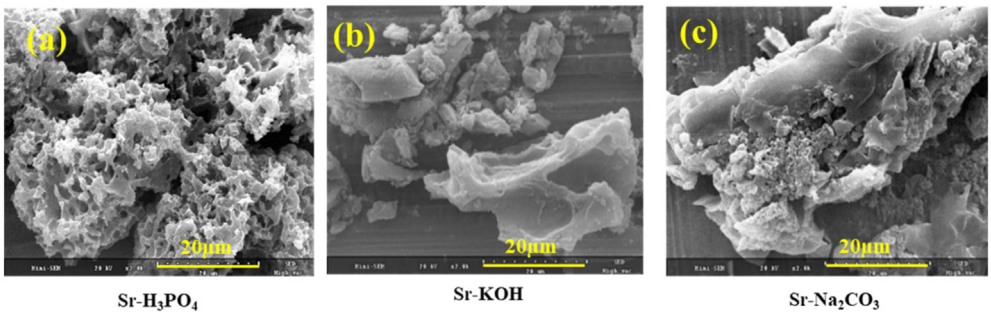

Figure 6. SEM images of (a) Sr–H_3PO_4 (b) Sr–KOH and (c) Sr–Na_2CO_3.

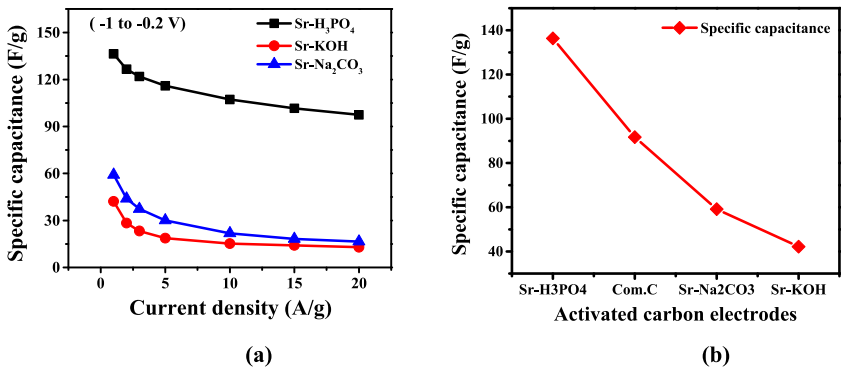

Figure 8. (a) Specific capacitance of three activated-carbon-electrodes as a function of current density.(b) Comparison of specific capacitance of three activated-carbon-electrodes along with commercial-activated-carbon electrode.

Table 4. Carbon-electrodes and their specific capacitance from GCD at different current densities.

S.N.	Activated-Carbon- electrodes	Specific capacitance C_{SP} (F/g) at different current densities						
		1 A/g	2 A/g	3 A/g	5 A/g	10 A/g	15 A/g	20 A/g
1	Sr–H_3PO_4	59.1	43.9	37.3	30.0	21.8	18.2	16.5
2	Sr–KOH	42.2	28.3	23.2	18.7	15.2	14.0	12.8
3	Sr–Na_2CO_3	136.3	126.5	121.9	115.9	107.2	101.5	97.3

electrode could be clearly perceived in Figure 8 b. and observed even higher than commercial-activated-carbon-electrode which was reported in our previous study [51].

3.7.3. Galvanostatic charge/discharge (GCD) studies of activated-carbon-electrodes

Galvanostatic charge/discharge (GCD) process is an analytical technique to calculate energy and power densities of the activated-carbon-electrodes. It provides the idea about the feasibility of applying these carbon for practical device fabrication.

Figure 9 shows the comparative charge discharge curves of Sr–H_3PO_4, Sr–KOH and Sr–Na_2CO_3-electrodes and commercial-activated-carbon-electrode at 1 A/g current density. One can see the equivalent and triangular shape charge discharge curves. Here the time taken for discharge was 60 s for Sr–KOH-electrode, 80 s for Sr–Na_2CO_3-electrode, 140 s for commercial carbon-electrode, whereas 210 s for Sr–H_3PO_4-electrode which is comparatively quite higher than Sr–KOH, Sr–Na_2CO_3 and commercial carbon electrodes respectively. The large discharge duration of Sr–H_3PO_4 may be due to high specific capacitance 136.3 F/g. The straight lines of charge/discharge curve and triangular shape further confirms the presence of EDLC behavior. It was also an indication of having low impurities and proper insertion between ACs and electrolyte ions [50] and again could be interconnected with high surface area 1269.5 m^2/g as well.

Here, we have calculated the energy and power densities of all three as prepared electrodes using Eqs. (2) and (3) [50]. A well-known "Ragone plot" is shown in Figure 10. In plot, one can clearly observe the outstripped energy density efficiency of the Sr–H_3PO_4 electrode than Sr–KOH and Sr–Na_2CO_3 electrodes which are clearly shown in Table 5. It was also obvious that Sr–H_3PO_4 electrode has maximum energy storage capability of 3.0 Wh/kg at a power density of 99.6 W/kg, demonstrating the faster charging ability (Table 5). So one can say that Sr–H_3PO_4 electrode is one of the potential candidates for EDLC application in supercapacitors. Energy and power densities are calculated by using Eqs. (2) and (3).

$$\mathbf{E} = \frac{1}{8} C_{SP} \Delta v^2 \tag{2}$$

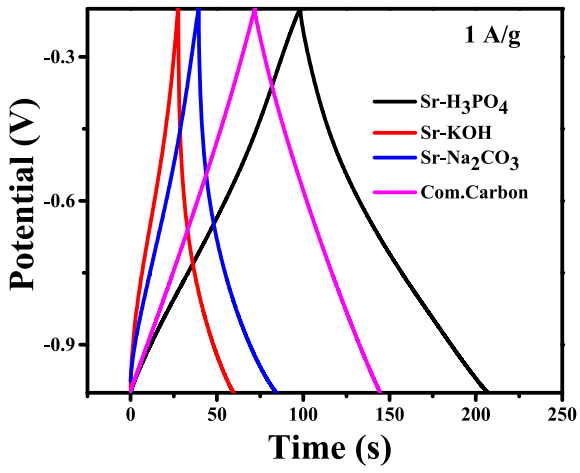

Figure 9. Comparison of GCD curves of Sr–H_3PO_4, Sr–KOH and Sr–Na_2CO_3 electrodes at 1A/g along with commercial carbon electrode.

$$\mathbf{P} = \frac{E}{\Delta t} \tag{3}$$

where, E is the energy density in Wh/kg, P is the power density in W/kg, Csp is the specific capacitance in F/g, ΔV is the potential window (V), whereas Δt (s) is the time of discharge.

3.7.4. Cyclic stability of activated carbon electrodes

Long life cycle is one of the vivacious characteristics that an ideal supercapacitor should have [50]. Figure 11 shows the life cycle assessment of three as prepared activated carbon electrodes. Here, 1000 cycles at a current densities of 3 A/g has been applied. It was found that the specific capacitance of the electrodes was slightly decreased at the beginning of cycle. However, it was found to be constant after 140 cycles. It was also observed that the specific capacitance was found to be dropped by 3.0 % for Sr–H_3PO_4-electrode, 10.6 % for Sr–KOH-electrode and 21.6% for Sr–Na_2CO_3-electrode after 1000 cycles (Table 5). This decay can be attributed to the decomposition of some electroactive

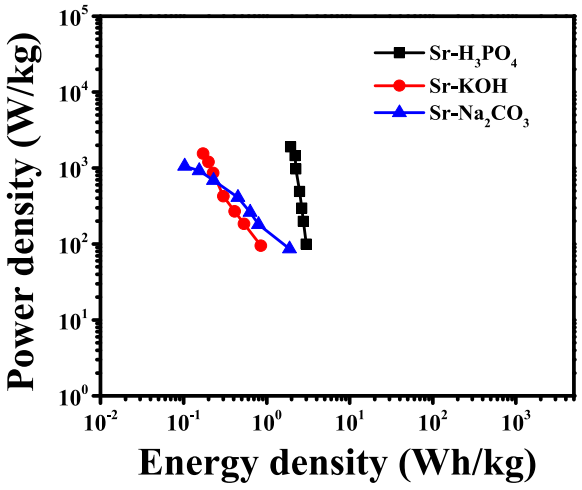

Figure 10. Ragone plots of Sr–H_3PO_4, Sr–KOH and Sr–Na_2CO_3 electrodes.

Table 5. Activated-carbon-electrode and their specific capacitance, Energy density, Power density, Capacity retention and ESR values.

S.N	Activated-carbon-electrodes	Specific Capacitance (F/g)	Energy density (Wh/Kg) at (1 A/g)	Power density (W/Kg) at (1 A/g)	Capacity retention %	ESR (Ω)
1	Sr–Na_2CO_3	59.1	1.8	95.1	78.4	0.6
2	Sr–KOH	42.1	0.8	95.2	89.4	0.5
3	Sr–H_3PO_4	136.3	3.0	99.6	96.9	0.4

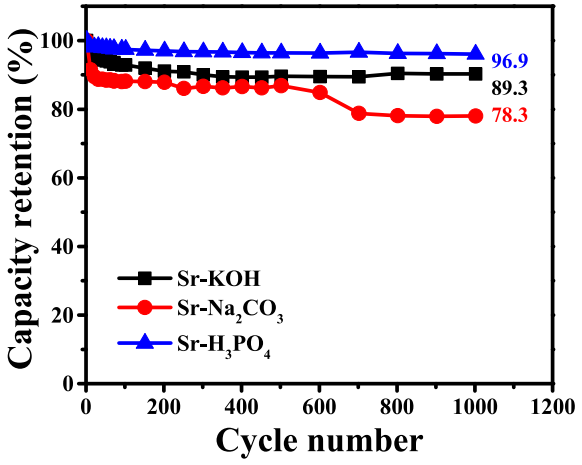

Figure 11. Long term cycling performance of Sr–H_3PO_4, Sr–KOH and Sr–Na_2CO_3 electrodes.

materials into the electrolyte during continuous charge/discharge assessment [52]. It revealed that Sr–H_3PO_4-electrode has excellent cycle stability than other 2 activated-carbon-electrodes. It may be due to high value of specific capacitance, high energy density and high % capacity retention of about 96.9 %. These aforesaid values might be due to enormous mesopores, along with micropores. These porosity not only improves the capacitance value but also increases the capacity retention/cyclic stability. However, Sarkar et al. has mentioned that some phosphorous group may remain on the surface which may contribute to enhance the capacitance by decreasing the surface hydrophobicity, and the metaphosphate which contributes to the stability of the capacitance [50]. Furthermore, its higher mesoporosity, facilitates the diffusion at higher current densities. Therefore, it could be resolved that both the specific capacitance and capacity retention can be improved by controlling the pore structure and phosphorus environment as well.

3.7.5. Electrochemical impedance spectroscopy (EIS) studies of activated carbon materials

Electrochemical impedance spectroscopy (EIS) is an important analytical technique to get information about the characteristic frequency response of supercapacitors and the capacitive phenomena occurring in the electrodes. The Nyquist impedance plots of the three different activated carbon electrodes are reported in Figure 12.

Figure 12 exhibited enlarged spectrum of Nyquist impedance plot. High frequency region of the plot displayed an incomplete semi circle whereas, low frequency region exhibited straight line curve. The semicircle curve of Nyquist impedance plot were associated with polarization resistance which reflects the diffusion or transport of electrolyte into the porous electrode material, while the straight verticle line was related to the capacitive behavior as described by Lu et al. [52] and Toupin et al [53].

The result implies that Sr–H_3PO_4-electrode, exhibited the highest conductivity or lowest internal resistance of about 0.4 Ω [53] than other two carbon electrodes namely Sr–KOH-electrode and Sr–Na_2CO_3-electrode (Table 5). This point attributed to high specific capacitance of Sr–H_3PO_4 electrode which significantly improves the ion diffusion and electron conduction procedure which has also been reflected by the higher power density of the Sr–H_3PO_4-electrode.

4. Conclusion

On the basis of results, following conclusions can be drawn.

The agro-waste, sawdust of *Shorea robusta* (Sal), can be used as good precursor materials for the production of nanoporous activated carbons. The carbonization temperature of 400 °C was found to be adequate to prepare phosphoric acid activated carbon (Sr–H_3PO_4), while this temperature was found to be insufficient for KOH and Na_2CO_3 activated carbon (Sr–KOH and Sr–Na_2CO_3).

Among the three ACs, H_3PO_4 activated carbon (Sr–H_3PO_4) showed best results in terms of porosity, surface area and electrochemical performances.

The overall electrochemical performance of Sr–H_3PO_4-electrode showed excellent capacitive behavior. The specific capacitance was found to be 136.3 F/g. The energy density was found to be 3.0 Wh/kg at power density of 99.6 W/kg, and low internal resistance of about 0.4 Ω. In the same way, cyclic stability was significantly high, 96.9 % after 1000 cycles of charge/discharge. Such type of behavior clearly indicates the

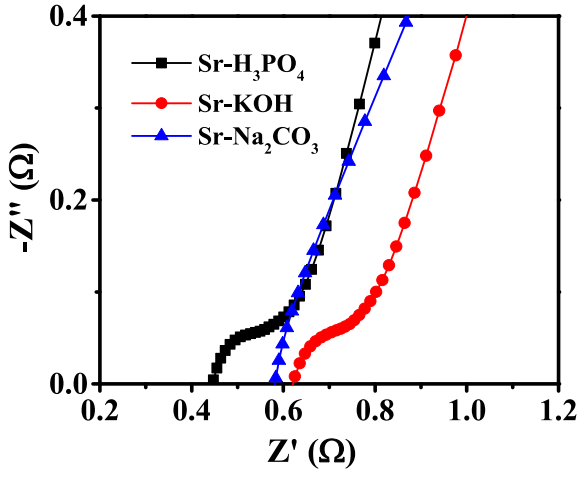

Figure 12. Nyquist plot of Sr–H_3PO_4, Sr–KOH and Sr–Na_2CO_3 electrodes at high frequency.

potentiality of the electrode for EDLC application in supercapacitive energy storage.

Declarations

Author contribution statement

Dibyashree shrestha: Performed experiments; Analysed the data; wrote the manuscript.

Armila Rajbhandari: Conceived and designed the experiments.

Funding statement

This research did not receive any specific grant from funding agencies in the public, commercial, or not-for-profit sectors.

Data availability statement

Data associated with this study has been deposited at Patan Multiple Campus, Tribhuvan University, Patan dhoka, Lalitpur, Nepal.

Declaration of interests statement

The authors declare no conflict of interest.

Additional information

No additional information is available for this paper.

Acknowledgements

Dibyashree Shrestha is thankful to "Institute of Science and Technology" (IOST), Tribhuvan University, Kirtipur, Kathmandu, Nepal for the Ph.D. study leave. The author is very grateful to Prof. Dr. Soo Wohn Lee of "Research Centre for Eco Multi-Functional Nano Material, Global Research Laboratory (GRL), Sun Moon University (SMU), South Korea" for providing laboratory facilities to carry out all advanced instrumental characterizations. Similarly, the author is thankful to Prof. Dr. Santi Maensiri of "School of Physics, Institute of Science, Suranaree University of Technology (SUT), Thailand for providing laboratory facilities to carry out electrochemical characterizations.

References

[1] J.M. Tarascon, Key challenges in future Li-battery research, Phil. Trans. Roy. Soc. France A368 (2010) 3227–3241.
[2] R. Kolz, M. Carlen, Principles and applications of electrochemical capacitors, Electrochem. Acta. 45 (2000) 2483–2498.
[3] B.E. Conway, Electrochemical supercapacitors; scientific fundamentals and technological applications, J. Electrochem. Soc. 138 (1991) 1539–1548.
[4] Z.J. Gao, L.Z. Wang, Graphene nanosheet/Ni^{2+}/Al^{3+} layered double-hydroxide composite as a novel electrode for a supercapacitor, Chem. Mater. 23 (15) (2011) 3509–3516.
[5] J. Wang, Z. Gao, Z. Li, Green synthesis of graphene nanosheets/ZnO composites and electrochemical properties, J. Solid State Chem. 184 (2011) 1421–1427.
[6] G. Wang, L. Zhang, J. Zhang, A review of electrode materials for electrochemical supercapacitors, Chem. Soc. Rev. 41 (2012) 797–828.
[7] W. Yang, Z. Gao, J. Ma, Controlled synthesis of Co_3O_4 and Co_3O_4@MnO_2 nanoarchitectures and their electrochemical capacitor application, J. Alloys Compd. 611 (2014) 171–178.
[8] Z. Gao, W. Yang, Y. Yan, J. Wang, J. Ma, X. Zhang, B. Zing, L. Liu, Synthesis and exfoliation of layered a-$Co(OH)_2$ nanosheets and their electrochemical performance for supercapacitors, Eur. J. Inorg. Chem. 27 (2013) 4832–4838.
[9] W. Yang, Z. Gao, N. Song, Synthesis of hollow polyaniline nano-capsules and their supercapacitor application, J. Power Sources 272 (2014) 915–921.
[10] A. Aworn, P. Thiravetyan, W. Nakbanpote, Preparation and characteristics of agricultural waste activated carbon by physical activation having micro- and mesopores, J. Anal. Appl. Pyrol. 82 (2) (2008) 279–285.
[11] E. Cetin, B. Moghtaderi, B.R. Gupta, T.F. Wall, Influence of pyrolysis conditions on the structure and gasification reactivity of biomass chars, Fuel 83 (2004) 2139–2150.
[12] M. Fan, W. Marshall, D. Daugard, R.C. Brown, Steam activation of chars produced from oat hulls and corn stover, Bioresour. Technol. 93 (2004) 103–107.
[13] P. Simon, Y. Gogotsi, Materials for electrochemical capacitors, Nat. Mater. 7 (2008) 845–854.
[14] A.M. Abioye, F.N. Ani, F. Nasir, Recent development in the production of activated carbon electrodes from agricultural waste biomass for supercapacitors: a review, Renew. Sustain. Energy Rev. 52 (2015) 1282–1293.
[15] M. Zhi, F. Yang, F. Meng, Effects of pore structure on performance of an activated-carbon supercapacitor electrode recycled from scrap waste tires, Sustain. Chem. Eng. 2 (7) (2014) 1592–1598.
[16] D.A. Ab, G. Hegde, Activated carbon nanospheres derived from bio-waste materials for supercapacitor applications – a review, RSC Adv. 5 (2015) 88339–88352.
[17] M. Olivares-Marin, J.A. Fernandez, M.J. Lazaro, Cherry stones as precursor of activated carbons for supercapacitors, Mater. Chem. Phys. 114 (1) (2009) 323–327.
[18] W. Chen, H. Zhang, Y. Huang, W. Wang, A fish scale based hierarchical lamellar porous carbon material obtained using a natural template for high performance electrochemical capacitors, J. Mater. Chem. 20 (2010) 4773–4775.
[19] D. Kalpana, S.H. Cho, S.B. Lee, Recycled waste paper – a new source of raw material for electric double-layer capacitors, J. Power Sources 190 (2) (2009) 587–591.
[20] J. Li, Q. Wu, Water bamboo-derived porous carbons as electrode materials for supercapacitors, New J. Chem. 39 (2015) 3859–3864.
[21] H. Sun, W. He, C. Zong, Template-free synthesis of renewable macroporous carbon via yeast cells for high performance supercapacitor electrode materials, Appl. Mater. Interfaces 5 (6) (2013) 2261–2268.
[22] K. Karthikeyan, S. Amaresh, S.N. Lee, Construction of high-energy-density supercapacitors from pine-cone-derived high-surface-area carbons, Chem. Sus. Chem. 7 (5) (2014) 1435–1442.
[23] K. Wang, N. Zhao, S. Lei, Promising biomass based activated carbons derived from willow catkins for high performance supercapacitors, Electrochim. Acta 166 (2015) 1–11.
[24] R. Wang, P. Wang, X. Yan, Promising porous carbon derived from celtuce leaves with outstanding supercapacitance and CO2 capture performance, Appl. Mater. Interfaces 4 (11) (2012) 5800–5806.
[25] C. Peng, X.B. Yan, R.T. Wang, Promising activated carbons derived from waste tea-leaves and their application in high performance supercapacitors electrodes, Electrochim. Acta 87 (2013) 401–408.
[26] X. Li, W. Xing, S. Zhuo, Preparation of capacitor's electrode from sunflower seed shell, Bioresour. Technol. 102 (2) (2011) 1118–1123.
[27] L. Jiang, J. Yan, L. Hao, High rate performance activated carbons prepared from ginkgo shells for electrochemical supercapacitors, Carbon 56 (2013) 146–154.
[28] D. Bhattacharjya, J.S. Yu, Activated carbon made from cow dung as electrode material for electrochemical double layer capacitor, J. Power Sources 262 (15) (2014) 224–231.
[29] W. Qian, F. Sun, Y. Xu, Human hair-derived carbon flakes for electrochemical supercapacitors, Energy Environ. Sci. 7 (2014) 379–386.
[30] H. Feng, M. Zheng, H. Dong, Three-dimensional honeycomb-like hierarchically structured carbon for high-performance supercapacitors derived from high ash-content sewage sludge, J. Mater. Chem. A. 3 (2015) 5225–15234.
[31] F. Cartula, M. Molina-Sabio, F. Rodriguez-Reinoso, Preparation of activated carbon by chemical activation with $ZnCl_2$, Carbon 29 (1991) 999–1007.
[32] H. Wang, Q. Hao, X. Yang, L. Lu, X. Wang, Graphene oxide doped polyaniline for supercapacitors, Electrochem. Commun. 11 (2009) 1158–1161.
[33] Z. Hu, M.P. Srinivasan, Y. Ni, Noval activation process for preparing highly microporous and mesoporous activated carbons, Carbon 39 (2001) 877–886.
[34] L.L. Zhang, X.S. Zhao, Carbon-based materials as supercapacitor electrodes, Chem. Soc. Rev. 38 (2009) 2520–2531.
[35] M. Molina-Sabio, F. Rodriguez-Reinoso, Role of chemical activation in the development of carbon porosity, J. Colloid. Surface. Physicochem. Eng. 241 (2004) 15–25.
[36] P. Simon, Y. Gogotsi, Capacitive energy storage in nanostructured carbon–electrolyte systems, Acc. Chem. Res. 46 (5) (2013) 1094–1103.
[37] W. Chaikittisilp, M. Hu, H. Wang, H.S. Huang, T. Fujita, K.C.W. Wu, L.C. Chin, Y. Yamauchi, K. Ariga, Nanoporous carbons through direct carbonization of a zeolitic imidazolate framework for supercapacitor electrodes, Chem. Commun. 58 (2012) 7259.
[38] H.L. Jiang, B. Liu, Y.Q. Lan, K. Kuratani, T. Akita, H. Shioyama, F. Zong, Q. Xu, From metal-organic framework to nanoporous carbon: toward a very high surface area and hydrogen uptake, J. Am. Chem. Soc. 133 (31) (2011) 11854–11857.
[39] K. Naoi, Nanohybrid capacitor: the next generation electrochemical capacitors, Fuel Cell 10 (5) (2010) 825–833.
[40] O. Rautiainen, Spatial yield model for Shorea robusta in Nepal, For. Ecol. Manag. 119 (1999) 151–162.
[41] D. Shrestha, G. Gyawali, A. Rajbhandari (Nyachhyon), Preparation and characterization of activated carbon from waste sawdust from saw mill, J. Inst. Sci. Technol. 22 (2018) 103–108.
[42] G. Wu, P. Tan, D. Wang, Z. Li, L. Peng, Y. Hu, C. Wang, W. Zhu, S. Chen, W. Chen, High-performance supercapacitors based on electrochemical-induced vertical-aligned carbon nanotubes and polyaniline nanocomposite electrodes, Sci. Rep. 7 (2017) 43676.
[43] J. Laine, A. Calafat, M. Labady, Preparation and characterization of activated carbons from coconut shell impregnated with phosphoric acid, Carbon 27 (1989) 191–195.
[44] N. Shimodaira, A. Masui, Raman spectroscopic investigations of activated carbon materials, J. Appl. Phys. 92 (2002) 902.
[45] M. Toupin, T. Brousse, D. Bélanger, Charge storage mechanism of MnO2 electrode used in aqueous electrochemical capacitor, Chem. Mater. 16 (2004) 3184–3190.

[46] D. Prahas, Y. Kartika, N. Indraswati, S. Ismadji, Activated carbon from jackfruit peel waste by H3PO4 chemical activation: pore structure and surface chemistry characterization, Chem. Eng. J. 140 (2008) 32–42.
[47] J. Wang, S. Kaskel, KOH activation of carbon-based materials for energy storage, J. Mater. Chem. 22 (45) (2012) 23710–23725.
[48] J.I. Kim, K.Y. Rhee, S.J. Park, Interactive effects of pore size control and carbonization temperatures on supercapacitive behaviors of porous carbon/carbon nanotube composites, J. Colloid Interface Sci. 377 (1) (2012) 307–312.
[49] K. Xie, M. Zhang, Y. Yang, L. Zho, W. Qu, Synthesis and supercapacitor performance of polyaniline/nitrogen-doped ordered mesoporous carbon composites, Nanos. Res. Lett. 13 (2018) 163.
[50] C.D. Lokhande, T.P. Gujar, V.R. Shinde, Electrochemical supercapacitor application of pervoskite thin films, Electrochem. Commun. 9 (2007) 1805–1809.
[51] D. Shrestha, S. Maensiri, U. Wongpratat, S.W. Lee, A. Rajbhandari, Nyachhyon, *Shorea robusta* derived activated carbon decorated with manganese dioxide hybrid composite for improved capacitive behaviors, J. Environ. Chem. Eng. 7 (2019) 103227.
[52] H. Lu, W. Dai, M. Zheng, N. Li, G. Ji, J. Cao, Electrochemical capacitive behaviors of ordered mesoporous carbons with controllable pore sizes, J. Power Sources 209 (2012) 243–250.
[53] M. Toupin, D. Bélanger, I.R. Hill, D. Quinn, Performance of experimental carbon blacks in aqueous supercapacitors, J. Power Sources 140 (2005) 203–210.